

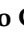





Article

Glyphosate-Based Herbicide Toxicophenomics in Marine Diatoms: Impacts on Primary Production and Physiological Fitness

Ricardo Cruz de Carvalho ^{1,2,*} , Eduardo Feijão ¹, Ana Rita Matos ^{3,4} , Maria Teresa Cabrita ⁵, Sara C. Novais ⁶, Marco F. L. Lemos ⁶ , Isabel Caçador ^{1,4}, João Carlos Marques ⁷, Patrick Reis-Santos ^{1,8} , Vanessa F. Fonseca ^{1,9}  and Bernardo Duarte ^{1,4} 

- ¹ MARE—Marine and Environmental Sciences Centre, Faculdade de Ciências da Universidade de Lisboa, Campo Grande, 1749-016 Lisbon, Portugal; emfeijao@fc.ul.pt (E.F.); micacador@fc.ul.pt (I.C.); pnsantos@fc.ul.pt (P.R.-S.); vffonseca@fc.ul.pt (V.F.F.); baduarte@fc.ul.pt (B.D.)
 - ² cE3c, Centre for Ecology, Evolution and Environmental Changes, Faculty of Sciences, University of Lisbon, Campo Grande, Edifício C2, Piso 5, 1749-016 Lisbon, Portugal
 - ³ BioISI—Biosystems and Integrative Sciences Institute, Plant Functional Genomics Group, Departamento de Biologia Vegetal, Faculdade de Ciências da Universidade de Lisboa, Campo Grande, 1749-016 Lisbon, Portugal; armatos@fc.ul.pt
 - ⁴ Departamento de Biologia Vegetal da Faculdade de Ciências da Universidade de Lisboa, Campo Grande, 1749-016 Lisbon, Portugal
 - ⁵ Centro de Estudos Geográficos (CEG), Instituto de Geografia e Ordenamento do Território (IGOT) da Universidade de Lisboa, Rua Branca Edmée Marques, 1600-276 Lisbon, Portugal; tcabrita@campus.ul.pt
 - ⁶ MARE—Marine and Environmental Sciences Centre, ESTM, Polytechnic of Leiria, 2411-901 Leiria, Portugal; sara.novais@ipleiria.pt (S.C.N.); marco.lemos@ipleiria.pt (M.F.L.L.)
 - ⁷ University of Coimbra, MARE—Marine and Environmental Sciences Centre, Department of Life Sciences, 3000 Coimbra, Portugal; jcmimar@ci.uc.pt
 - ⁸ Southern Seas Ecology Laboratories, School of Biological Sciences, The University of Adelaide, Adelaide, SA 5005, Australia
 - ⁹ Departamento de Biologia Animal da Faculdade de Ciências da Universidade de Lisboa, Campo Grande, 1749-016 Lisbon, Portugal
- * Correspondence: rfcruz@fc.ul.pt

Received: 9 September 2020; Accepted: 19 October 2020; Published: 22 October 2020



Featured Application: Application of non-invasive bio-optical techniques to evaluate the ecotoxicity of glyphosate-based pesticide in marine diatoms with confirmation by classical biochemical tools.

Abstract: Glyphosate is the main active component of the commercial formulation Roundup[®], the most widely used chemical herbicide worldwide. However, its potential high toxicity to the environment and throughout trophic webs has come under increasing scrutiny. The present study aims to investigate the application of bio-optical techniques and their correlation to physiological and biochemical processes, including primary productivity, oxidative stress, energy balance, and alterations in pigment and lipid composition in *Phaeodactylum tricornutum*, a representative species of marine diatoms, using the case study of its response to the herbicide glyphosate-based Roundup[®] formulation, at environmentally relevant concentrations. Cultures were exposed to the herbicide formulation representing effective glyphosate concentrations of 0, 10, 50, 100, 250, and 500 $\mu\text{g L}^{-1}$. Results showed that high concentrations decreased cell density; furthermore, the inhibition of photosynthetic activity was not only caused by the impairment of electron transport in the thylakoids, but also by a decrease of antioxidant capacity and increased lipid peroxidation. Nevertheless, concentrations of one of the plastidial marker fatty acids had a positive correlation with the highest concentration as well as an increase in total protein. Cell energy allocation also increased with concentration, relative to control and the lowest concentration, although culture growth was

inhibited. Pigment composition and fatty acid profiles proved to be efficient biomarkers for the highest glyphosate-based herbicide concentrations, while bio-optical data separated controls from intermediate concentrations and high concentrations.

Keywords: photobiology; energetic metabolism; pesticide; oxidative stress; glyphosate

1. Introduction

In recent years, the concern over emerging pollutants and their effects on the marine biota metabolism has grown exponentially. Man-made contaminants invariably present new challenges in monitoring efforts and risk prevention [1]. These chemicals, including pesticides, pharmaceuticals, and personal and household care products, are used daily worldwide and their presence in the environment stems from an exponential increase in human activities related to their usage [2]. In the first decade of the 21st century, more than 50% of the total production of chemicals included environmentally harmful compounds [3]. Furthermore, the speed of technological advances made in synthetic chemical production continues to increase the list of these novel substances [4], raising important questions and concerns about their ecotoxicity and efficient monitoring methodologies.

Glyphosate (N-(phosphonomethyl) glycine) is a phosphonate herbicide and the main active ingredient in the commercial mixture Roundup[®], the most used chemical herbicide worldwide [5,6]. Glyphosate is a broad-spectrum herbicide with a unique mode of action: It acts as a glycine analogue, inhibiting the enzyme 5-enolpyruvyl-shikimate-3-phosphate synthase (EPSPS) of the shikimate pathway, thus affecting the synthesis of aromatic amino acids [7]. The dramatic increase in its use globally is also associated with the development of glyphosate-tolerant crops that present a tolerant EPSPS synthase and/or a glyphosate metabolism gene [8]. Being relatively unsusceptible to chemical- and photodecomposition, glyphosate can easily reach coastal and marine areas via a multitude of direct and/or diffuse pathways [9]. While pesticides are mainly used in both agriculture and weed control, their persistence in any given aquatic environment can allow them to be carried into remote marine environments, although the exact means by which this occurs is still a subject under debate [10,11].

Marine phytoplankton is a key biomonitor in many marine trophic webs which, under natural conditions, responds to a wide range of environmental disturbances and contamination events [12–16] and any impacts at this level are highly likely to lead to bottom-up impacts. Glyphosate was shown to impair cyanobacteria growth at concentrations as low as 50 $\mu\text{g L}^{-1}$ [17], and in freshwater, glyphosate influences microbial community structure, changing the community from green algae and diatoms (glyphosate sensitive) to cyanobacteria (glyphosate tolerant) [18,19]. Moreover, structural changes to marine communities have been associated with glyphosate application [20]. Ultimately, ecotoxicological studies on marine organisms are of the utmost importance to establish guidelines to safeguard local biodiversity and the functioning of estuarine, coastal, and marine environments [21,22].

Diatoms, as part of phytoplankton, are among the first organisms to be affected by contaminants, quickly responding to suspended toxicants due to their small size (0.2–200 μm) and high uptake rates [13,23–26]. Diatoms are also constantly re-adjusting the equilibrium between energy production from photosynthesis and energy consumption under environmental stress conditions, an ability that undermines their success in highly dynamic coastal and estuarine environments [27]. While they are responsible for half of all the photosynthesis on Earth and thus have an important role in the global biological carbon pump and the silica cycle [28], our knowledge of carbon allocation regulation in diatoms is very limited, particularly because of these present distinct metabolic compartmentations and additional metabolic pathways in comparison to the more widely studied green algae [29–32].

Diatoms are also major marine producers of specific fatty acids [32], including essential fatty acids (EFA), linoleic acid (omega-6 [ω -6] class), and α -linolenic acid (ALA). Diatoms also produce long-chain polyunsaturated fatty acids (LC-PUFA) such as eicosapentaenoic acid (EPA) and docosahexaenoic acid

(DHA) (omega-3 [ω -3] class) [33]. Vertebrates cannot synthesize essential fatty acids and the ability to produce LC-PUFA is also limited; they do not obtain these through their diet [34,35]. Furthermore, LC-PUFA plays key roles in animal and human health, being major components of neurological tissues [36].

Photosynthesis has been shown to be impaired by glyphosate-based herbicides within wide ranges of concentrations, including in cordgrass *Spartina densiflora* from spray application at concentrations of 720–7200 g ha⁻¹ [37], to direct contact of 10–80 mg L⁻¹ in *Anabaena fertilissima* [38]. In both cases, there was inhibition of CO₂ assimilation and depletion of intermediates from the photosynthetic carbon reduction cycle due to deregulation of the shikimate pathway [39,40]. In such scenarios, non-invasive high-throughput bio-optical screening tools, such as Pulse Amplitude Modulated (PAM) fluorometry, emerge as invaluable techniques to evaluate ecotoxicity in photosynthetic organisms [12,41,42]. Through PAM it is possible to translate the fluorescence signals as proxies to the bioenergetics involved in photosynthesis in a non-destructive form [13,41–44] to efficiently assess primary productivity [45,46] and the physiological effects in plant material at different concentrations of contaminants [12,41,42,44].

The half-life of glyphosate in water varies between 45 and 60 days [47] and phytoplankton have a fast response in the presence of contaminants [13,25]. Thus, it is of the utmost importance to evaluate the potential effects of glyphosate in the environment, namely on primary producers. The present study aimed to correlate bio-optical data with the ecotoxicological effects of the exposure of the glyphosate-based herbicide Roundup[®] (i.e., currently found in estuarine and marine systems) [48–51], with the working hypothesis that, similarly to other photosynthetic organisms, this herbicide will have a negative impact on primary productivity, antioxidant enzyme activity, energy balance, pigment and fatty acid composition of the model diatom *Phaeodactylum tricorutum*, and its potential implications on estuarine or coastal marine ecosystems.

2. Materials and Methods

2.1. Experimental Setup

The model diatom *P. tricorutum* Bohlin (Bacillariophyceae) (IO 108–01, IPMA, ALISU—Algae Collection of the University of Lisbon, Lisbon, Portugal) was harvested from monoclonal cultures in 250 mL of f/2 medium [52] in culture flasks (Drechsel-type gas washing bottles) under controlled conditions for 4 days (18 ± 1 °C, under constant aeration and a 14 h light/10 h dark photoperiod). The growth chamber was programmed to simulate sunrise and sunset using a sinusoidal function with a light intensity at noon simulating a natural light environment (RGB 1:1:1, Maximum PAR 80 μmol photons m⁻² s⁻¹, 14/10 h day/night rhythm). According to the Organization for Economic Cooperation and Development (OECD) guidelines for algae bioassays [53] and the recommended initial cell density for microalgae cells with similar size to *P. tricorutum*, initial cell concentration was approximately 2.7 × 10⁵ cells mL⁻¹. Forty-eight hours after inoculation, cultures were exposed to 0, 10, 50, 100, 250, or 500 μg L⁻¹ glyphosate for 48 h [24,41,46], obtained from the glyphosate-based herbicide “Roundup[®] Pronto” containing 7.2 g L⁻¹ of glyphosate. Since no studies have measured glyphosate in marine water, the herbicide concentrations were chosen based on the range of environmental concentrations found in agricultural water streams in relevant literature [49–52], as it was found that this chemical presents the same half-life in saltwater as it does in freshwater [10,11]. While other substances compose Roundup[®], glyphosate is the main active component. Exposure took place 48 h after inoculation to ensure that the experiment was performed during the cell exponential growth phase [24,41,46]. There were three replicates for each herbicide concentration from a total of 18 experimental units. To avoid contamination, the labware was washed with HNO₃ (20%) for 48 h, rinsed thoroughly with ultra-pure water and autoclaved. All culture manipulations were performed in a laminar airflow chamber using aseptic techniques.

2.2. Growth Rates and Cell Harvesting

During the exposure trials, daily cell counting of *P. tricornutum* subjected to different glyphosate-based herbicide concentrations was performed using a Neubauer improved counting chamber, with an Olympus BX50 (Tokyo, Japan) inverted microscope, at 400-times magnification. Culture growth was determined from the difference between initial and final logarithmic cell densities divided by the exposure period [54], expressed as the mean specific growth rate per day. Samples for photochemical and biochemical analysis were collected after 48 h of exposure to glyphosate-based herbicide (4 days after inoculation). Based on the glyphosate-based herbicide concentrations, we determined the No Observed Effect Concentration (NOEC) and the Lowest Observed Effect Concentration (LOEC) [55]. Furthermore, by application of a sigmoidal dose-response curve to the endpoint measurement for each exposure concentration, we also determined the Effective Concentration (EC) which inhibited growth by 10% (EC₁₀), 25% (EC₂₅), and 50% (EC₅₀) [55]. At the end of the exposure time and after the chlorophyll fluorescence measurements (see next section), samples of 30 mL of culture were centrifuged at 4000× g for 15 min at 4 °C (Sigma 2-16K, Sigma Laborzentrifugen GmbH, Germany). The supernatant was removed, and pellets were immediately frozen in liquid nitrogen and stored at −80 °C until analysis.

2.3. Bio-Optical Assessment through Chlorophyll a Pulse Amplitude Modulated (PAM) Fluorometry

Pulse amplitude modulated (PAM) chlorophyll fluorescence measurements were performed using a FluorPen FP100 (Photo System Instruments, Drasov, Czech Republic) on 15 min dark-adapted samples using a 1 mL cuvette. Culture cell density was assessed daily, using a non-actinic light to measure minimum chlorophyll fluorescence (F₀). Analysis of chlorophyll transient light curves (Kautsky plot) was carried out using the OJIP test according to [41]. Fluorometric analysis parameters and their description can be accessed in Table 1.

Table 1. Fluorometric analysis parameters and their description.

OJIP Test	
Area	Corresponds to the oxidized quinone pool size available for reduction and is a function of the area above the Kautsky plot
N	Reaction center turnover rate
S _M	Corresponds to the energy needed to close all reaction centers
M ₀	Net rate of PS II RC closure
γ _{RC}	Probability that a PS II chlorophyll molecule will function as an RC
P _G	Grouping probability between the two PS II units
ABS/CS	Absorbed energy flux per cross-section
TR/CS	Trapped energy flux per cross-section
ET/CS	Electron transport energy flux per cross-section
DI/CS	Dissipated energy flux per cross-section
RC/CS	Number of available reaction centers per cross-section
TR ₀ /DI ₀	Contribution or partial performance due to the light reactions for primary photochemistry
δ _{R0} /(1 − δ _{R0})	Contribution of PS I, reducing its end acceptors
ψ ₀ /(1 − ψ ₀)	Contribution of the dark reactions from Q _A [−] to PC
ψ _{E0} /(1 − ψ _{E0})	Equilibrium constant for the redox reactions between PS II and PS I
RE ₀ /RC	Electron transport from PQH ₂ to the reduction of PS I end electron acceptors
RC/ABS	Reaction center II density within the antenna chlorophyll bed of PS II

2.4. Pigment Analysis

Pigment extraction was performed according to methodologies from previous works [12,13,46]. Pure acetone was added to sample pellets and maintained in an ultra-sound cold bath for 2 min, ensuring total disaggregation of cell material, and kept in the dark at $-20\text{ }^{\circ}\text{C}$ for 24 h to prevent degradation. Samples were centrifuged for 15 min at $4000\times g$ and $4\text{ }^{\circ}\text{C}$ and the supernatants were scanned by a dual-beam spectrophotometer from 350 nm to 750 nm at 0.5 nm steps (Shimadzu UV-1603, Shimadzu Co., Kyoto, Japan). Using the SigmaPlot Software, the absorbance spectrum was introduced in the Gauss-Peak Spectra (GPS) fitting library. Pigment analysis was performed according to [56], allowing the detection of chlorophyll *a* and *c*, pheophytin *a*, β -carotene, fucoxanthin, diadinoxanthin (DD), and diatoxanthin (DT).

2.5. Antioxidant Enzyme Assays

The soluble protein fraction was extracted at $4\text{ }^{\circ}\text{C}$ from cell pellets in 1 mL of 50 mM sodium phosphate buffer (pH 7.6) with 0.1 mM Na-EDTA and placed in an ultrasound bath for 1 min from the previously collected pellets. The homogenate was centrifuged at $10,000\times g$ for 10 min at $4\text{ }^{\circ}\text{C}$ to remove debris and the supernatant collected to a new tube. Protein concentration was determined according to [57]. Catalase (CAT) activity was measured according to [58], monitoring H_2O_2 consumption and the consequent decrease in absorbance at 240 nm ($\epsilon = 39.4\text{ mM}^{-1}\text{ cm}^{-1}$). The reaction mixture contained 50 mM of sodium phosphate buffer (pH 7.6), 0.1 mM of Na-EDTA, and 100 mM of H_2O_2 with the reaction being started by the addition of 100 μL of extract. Ascorbate peroxidase (APX) was assayed according to [59]. The reaction mixture contained 50 mM of sodium phosphate buffer (pH 7.0), 5 μM of H_2O_2 , and 0.25 μM L-ascorbate, and the reaction was also initiated with the addition of 100 μL of the extract. The activity was recorded as the decrease in absorbance at 290 nm and the amount of ascorbate oxidized calculated from the molar extinction coefficient ($\epsilon = 2.8\text{ mM}^{-1}\text{ cm}^{-1}$). Superoxide dismutase (SOD) activity was assayed according to [60] by monitoring the reduction of pyrogallol at 325 nm. The reaction mixture contained 50 mM of sodium phosphate buffer (pH 7.0) and 0.24 mM of pyrogallol and ultra-pure water, with the reaction being started by the addition of 10 μL of extract. Control assays were done in the absence of substrate to evaluate the autoxidation of the substrates. All the assays were performed at $25\text{ }^{\circ}\text{C}$ in a UV500 UV-Visible Spectrometer (Unicam, Waltham, MA, USA).

2.6. Lipid Peroxidation Analysis

Lipid peroxidation products were determined according to [61]. Sample pellets were homogenized briefly in 1.5 mL of 10% (*v/v*) Trichloroacetic acid (TCA), containing 0.4% (*w/v*) thiobarbituric acid (TBA) and placed in an ultrasound bath for 1 min. The reaction was conducted at $100\text{ }^{\circ}\text{C}$ for 30 min; immediately after it was halted through placement in ice, and after centrifugation at $15,000\times g$ for 10 min at $4\text{ }^{\circ}\text{C}$, 1 mL of the supernatant was collected and mixed with 1 mL of 0.4% TBA and incubated again under the same conditions. After again cooling down in ice and centrifuging, the absorbance at 532 nm and 600 nm of the supernatant was recorded by spectrophotometry. The concentration of malondialdehyde (MDA) was determined using the molar extinction coefficient ($\epsilon = 155\text{ mM}^{-1}\text{ cm}^{-1}$).

2.7. Fatty Acid Profiles

The fatty acid analysis was performed according to [46] by direct trans-esterification of sample pellets, in freshly prepared methanol sulfuric acid (97.5:2.5, *v/v*), at $70\text{ }^{\circ}\text{C}$ for 60 min, using the internal standard pentadecanoic acid (C15:0). Fatty acid methyl esters (FAMES) were recovered using petroleum ether, dried with an N_2 flow, and re-suspended in an adequate amount of hexane. Through gas chromatography (Varian 430-GC gas chromatograph equipped with a hydrogen flame ionization detector set at $300\text{ }^{\circ}\text{C}$, Middelburg, The Netherlands), 1 μL of the FAME solution was analyzed, setting the injector temperature to $270\text{ }^{\circ}\text{C}$, with a split ratio of 50. The fused-silica capillary column (50 m \times 0.25 mm; WCOT Fused Silica, CP-Sil 88 for FAME; Varian, Middelburg, The Netherlands)

was maintained at a constant nitrogen flow of 2.0 mL min⁻¹ and the oven set to 190 °C. Fatty acids identification was performed by comparison of retention times with standards (Sigma-Aldrich) and chromatograms analyzed by the peak surface method, using the Galaxy software. To determine the membrane saturation levels, the double bond index (DBI) was calculated according to [46]:

$$DBI = \frac{2 \times (\% \text{ monoenes} + 2 \times \% \text{ dienes} + 3 \times \% \text{ trienes} + 4 \times \% \text{ tetraenes} + 5 \times \% \text{ pentaenes})}{100} \quad (1)$$

2.8. Energy Balance

Cell pellets were homogenized by ultrasonication on ice (3x 10s at A = 20%) using 1 mL of Milli-Q water. Aliquots were taken from each sample for the analysis of lipid, carbohydrate and protein contents, and electron transport system (ETS) activity. In all assays, ultrapure water was used as reaction blank. The spectrophotometric measurements were performed in triplicates, at 25 °C, using a synergy H1 Hybrid Multi-Mode microplate reader (Biotek[®] Instrument, Winooski, VT, USA).

2.8.1. Energy Available

The energy available (Ea) was measured by determining the total protein, carbohydrate, and lipid contents and transforming the results into energetic equivalents (combustion energies: 17,500 mJ mg carbohydrates⁻¹, 24,000 mJ mg protein⁻¹, and 39,500 mJ mg lipid⁻¹) [61]. Extraction and quantification of total lipids, proteins, and carbohydrates were performed according to [62,63] with minor modifications [64]. Cell pellets were resuspended in 50 mM sodium phosphate buffer (pH 7) containing 1 mM phenylmethylsulfonyl fluoride (PMSF). Cell disruption was performed with 0.42–0.6 mm glass beads (Sigma-Aldrich) for 15 min at 6.5 ms⁻¹ (FastPrep-24, MP Biomedicals). Cell extract was centrifuged at 10,000× g for 20 min at 4 °C. The supernatant was stored at –80 °C until further analysis. Total protein content in the samples was determined using Bradford's method [56]. Total lipids were extracted by adding 250 µL of chloroform (spectrophotometric grade, Sigma-Aldrich), 250 µL of methanol (spectrophotometric grade, Sigma-Aldrich) and 125 µL Milli-Q water to 150 µL of the sample. After centrifugation at 1000× g for 5 min, the organic phase and interphase were removed and 500 µL of H₂SO₄ was added to 100 µL of lipid extract and charred for 15 min at 200 °C. The mixture was cooled down to 20 °C, 1.5 mL of deionized water was added, and total lipid content was determined by measuring the absorbance at 375 nm and compared to a calibration curve using tripalmitin values as standard. Total carbohydrate content was determined by adding 50 µL of 15% TCA to the 150 µL of sample and subjected to –20 °C for 10 min. After centrifugation at 1000× g for 10 min, the total carbohydrate content of the supernatant fraction was quantified by adding 50 µL of 5% (v/v) phenol and 200 µL of 18 M H₂SO₄ to 50 µL extract [65]. Following 30 min of incubation at 20 °C, absorbance was measured at 492 nm and compared to a calibration curve using glucose as standard.

2.8.2. Energy Consumption

Cellular oxygen consumption and metabolism are directly linked to mitochondrial ETS activity. As such, ETS was determined according to [66] with major modifications [65]. In 30 µL of sample or blank, 20 µL of homogenizing buffer [0.3 M Tris, 15% (w/v) polyvinyl pyrrolidone (PVP), 459 µM MgSO₄, 1.5 mL Triton X-100, pH 8.5], 100 µL of buffered substrate solution (reduced nicotinamide adenine dinucleotide (NADH) (1.79 mM) and reduced nicotinamide adenine dinucleotide phosphate (NADPH) (280 µM) in 0.13 M Tris, 0.3% (w/v) Triton X-100, pH 8.5) were added. The reaction was initiated by adding 50 µL of 8 mM p-iodonitrotetrazolium (INT), following the change in absorbance at 490 nm over a 3 min period at 20 °C. The formazan formed was calculated by using the extinction coefficient, $\epsilon = 15,900 \text{ mM}^{-1} \text{ cm}^{-1}$.

The cellular energy consumption (Ec) was determined by using the ETS data (for each 2 µmol of INT-formazan formed, 1 µmol of O₂ was consumed in the ETS), transforming the calculated quantity

of oxygen consumed into energetic equivalents by using the specific oxyenthalpic equivalents for an average lipid, protein, and carbohydrate mixture of 480 kJ mol O₂⁻¹ [62].

2.8.3. Cellular Energy Allocation

The cellular energy allocation (CEA), a methodological approach that integrates the energy available and energy consumption of an organism, was standardized to 10⁶ cells and calculated based on measurements of lipid, carbohydrate, and protein content and ETS activity for each sample as follows [67]:

$$CEA = \frac{Ea}{Ec} \quad (2)$$

where:

$$Ea \text{ (available energy)} = \text{carbohydrate} + \text{lipid} + \text{protein} \text{ (mJ } 10^{-6} \text{ cells)} \quad (3)$$

$$Ec \text{ (energy consumption)} = \text{ETS activity} \text{ (mJ h}^{-1} \text{ } 10^{-6} \text{ cells)} \quad (4)$$

2.9. Statistical Analysis

Each variable was evaluated through one-way ANOVA with Tukey's multiple comparisons test (GraphPad Prism 6.03 for Windows, GraphPad Software, San Diego, CA, USA), regarding differences among glyphosate-based herbicide concentrations. The data obtained from the Kautsky plots, pigment, and fatty acid profiles, were used as the basis for the construction of the respective resemblance matrixes based on the Euclidean distances between samples. To classify and separate the different treatment groups, statistical multivariate models based on the Kautsky plot, pigment composition, and fatty acid profile variable were generated using Canonical Analysis of Principal Coordinates (CAP), through the non-parametric multivariate analysis packages in Primer 6 software as described previously in other works [12,45,68,69].

3. Results

3.1. Cell Growth Rates

Regarding cell density, after 48 h exposure *P. tricornutum* cultures were negatively affected, in particular by the two highest concentrations of glyphosate-based herbicide (250 and 500 µg L⁻¹), with slight decreases in cell density observed only at lower concentrations (50 and 100 µg L⁻¹) (Figure 1A).

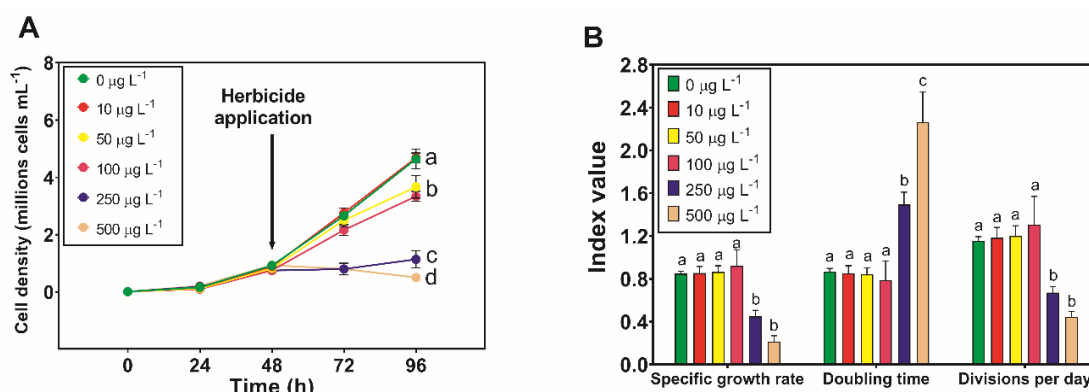


Figure 1. Growth indicators ((A) cell density and (B) derived growth parameters) of *Phaeodactylum tricornutum* following exposure to a herbicide formulation representing different glyphosate-based herbicide concentrations for (A) 24 h and 48 h, and (B) 48 h (mean ± s.d., n = 3, different letters indicate significant differences at $p < 0.05$).

However, after 48 h exposure only decreases in specific growth rates, with lower divisions per day and higher doubling time, were observed at the highest glyphosate-based herbicide concentrations ($>250 \mu\text{g L}^{-1}$) (Figure 1B). Therefore, a negative effect was observed in the two highest herbicide formulation concentrations regarding all the determined growth parameters. Based on the glyphosate-based herbicide concentrations present in the environment surrounding the diatom population used in the experiment, we determined the respective NOEC ($10 \mu\text{g L}^{-1}$), the LOEC ($50 \mu\text{g L}^{-1}$), the EC₁₀ ($15.4 \mu\text{g L}^{-1}$), the EC₂₅ ($94.4 \mu\text{g L}^{-1}$), and the EC₅₀ ($225.9 \mu\text{g L}^{-1}$).

3.2. Bio-Optical Assessment of Diatom Photochemistry

Apart from the lowest concentration ($10 \mu\text{g L}^{-1}$), the Kautsky plots showed decreasing fluorescence values with increasing herbicide quantities (Figure 2), particularly at the highest glyphosate-based herbicide concentrations (250 and $500 \mu\text{g L}^{-1}$).

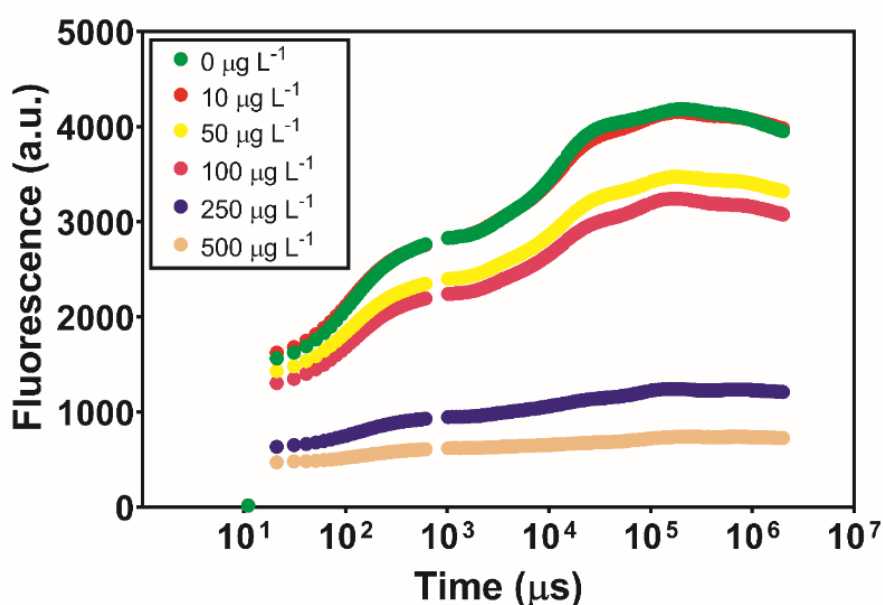


Figure 2. Chlorophyll transient kinetics (OJIP curves) in *Phaeodactylum tricorutum* following a 48 h exposure to a glyphosate-based herbicide formulation in different concentrations (mean \pm s.d., $n = 3$).

The analysis of the photochemical process from light-harvesting electronic transport, represented by the four main energy fluxes, demonstrates the effects of exposure of the different herbicide concentrations in *P. tricorutum* cultures (Figure 3).

The amount of energy absorbed by the photosystem II (PS II) antennae (ABS/CS), the energy flux that was effectively trapped inside the PS II (TR/CS) and transported within the electron transport chain (ETC) (ET/CS), as well as in the energy dissipation flux (DI/CS) and the reduction of the number of oxidized PS II reaction centers (RC/CS), all showed the same pattern with increasing concentrations. Overall, no effects relative to the control were observed at the lowest glyphosate-based herbicide concentration ($10 \mu\text{g L}^{-1}$), but a small decreasing effect of intermediate concentrations (50 and $100 \mu\text{g L}^{-1}$) and a high decrease in the highest glyphosate-based herbicide concentrations (250 and $500 \mu\text{g L}^{-1}$) was evident. These changes can be further analyzed through inspection of the functioning of different components of the photosystems and ETC in response to glyphosate-based herbicide concentration (Supplementary Figure S1). Regarding the oxidized quinone pool size, there was a decrease only in the highest glyphosate-based herbicide concentrations (250 and $500 \mu\text{g L}^{-1}$). However, there were no significant changes in the number of Q_A redox turnovers until maximum fluorescence was reached (N), except for the highest concentration in which enhancement was observed. The same pattern occurred in the energy needed to close (reduce) all RCs (S_M). At the highest glyphosate-based

herbicide exposure concentrations (250 and 500 $\mu\text{g L}^{-1}$), a decrease in the probability of a PS II chlorophyll molecule functioning as an RC (γ_{RC}) was detected. However, no differences were observed in the Q_{A} reduction rate (M_0).

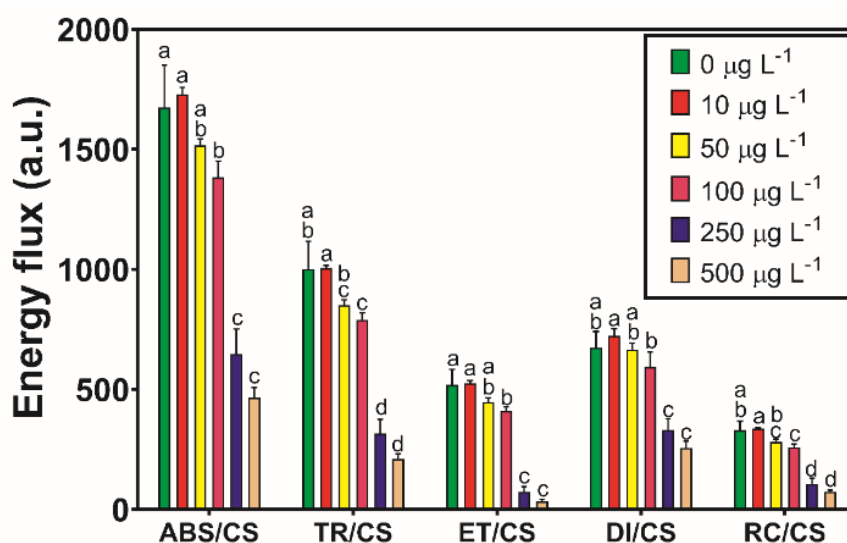


Figure 3. The energy fluxes (absorbed (ABS/CS), trapped (TR/CS), transported (ET/CS) and dissipated (DI/CS)) and the number of available reaction centers per cross-section (RC/CS) in *Phaeodactylum tricornutum* following a 48 h exposure to a glyphosate-based herbicide formulation in different concentrations (mean \pm s.d., $n = 3$, different letters indicate significant differences at $p < 0.05$).

While the active OECs showed a decrease only under the highest glyphosate-based herbicide concentration (500 $\mu\text{g L}^{-1}$), the P_G , the grouping probability that correlates with the disconnection between the two PS II units, increased with the highest glyphosate-based herbicide concentration (250 and 500 $\mu\text{g L}^{-1}$) (Figure 4).

Between PS II and PS I, photochemical processes showed a significant decrease in the contribution of light (TR_0/DI_0) and dark ($\psi_0/1 - \psi_0$) reactions of the photochemical cycle in the highest glyphosate-based herbicide concentration (250 and 500 $\mu\text{g L}^{-1}$). A similar pattern was observed in the reaction center density within the PS II antenna chlorophyll bed (RC/ABS). On the other hand, at the PS I level there was a significant enhancement in the activity of this photosystem ($\delta_{\text{R}0}/1 - \delta_{\text{R}0}$) in response to the highest glyphosate-based herbicide concentrations, also leading to an increase in the equilibrium constant for the redox reaction between both photosystems towards the PS II ($\psi_{\text{E}0}/(1 - \psi_{\text{E}0})$). Furthermore, regarding PS I, intrinsic changes led, in turn, to an increase of the electron transport from PQH_2 to the reduction of the PS I end acceptors (RE_0/RC).

In the rapid light curve (RLC)-derived parameters, the photosynthetic efficiency (α) and the maximum electron transport rate (ETR_{max}) only decreased with the highest glyphosate-based herbicide concentration (500 $\mu\text{g L}^{-1}$), with no effect on photoinhibition (β) and light saturation (E_k), with only a slight reduction at 250 $\mu\text{g L}^{-1}$ glyphosate-based herbicide exposure in the latter parameter (Supplementary Figure S2).

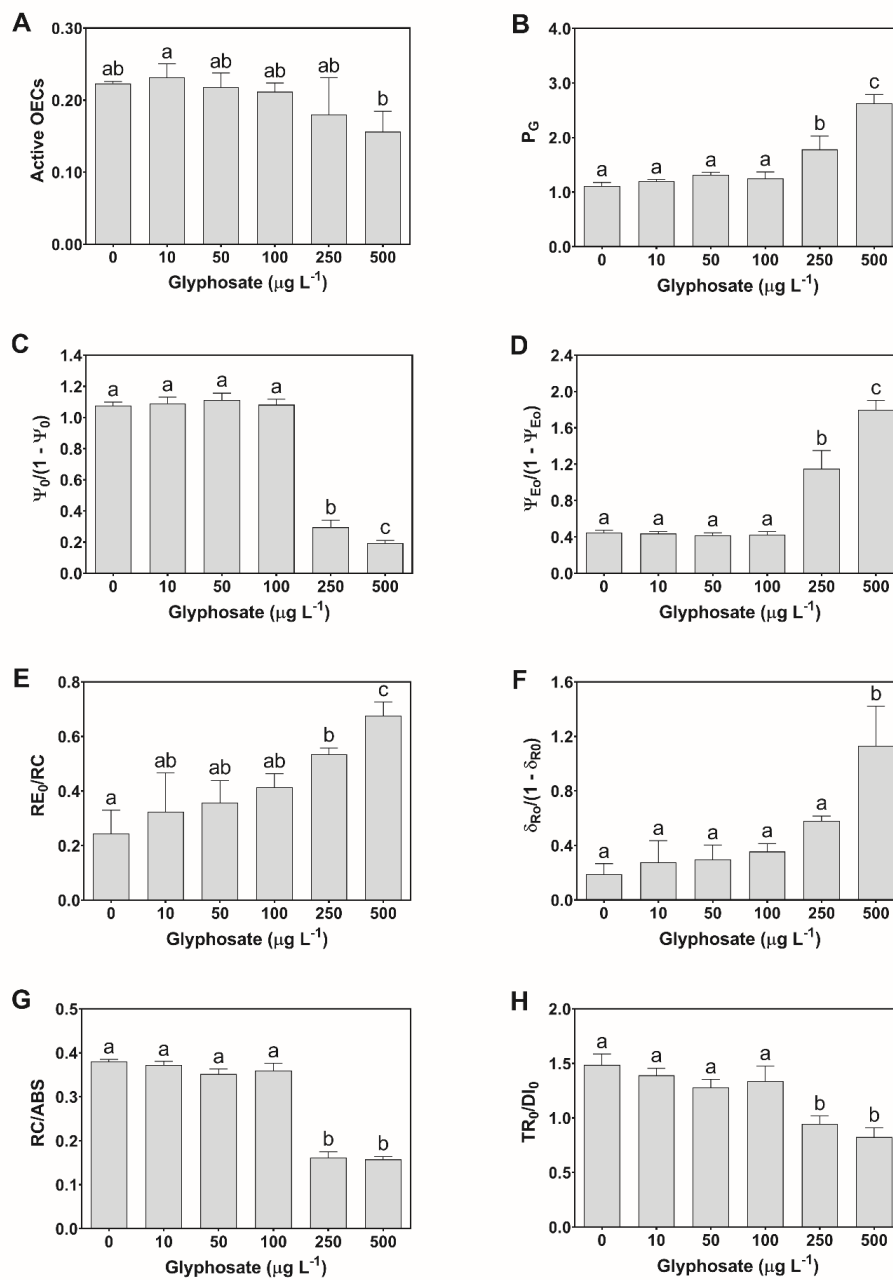


Figure 4. Photosystems I (PS I) and II (PS II) photochemical traits (A), active oxygen-evolving complexes (OECs); (B), grouping probability between the two PS II units (P_G); (C), the contribution of the dark reactions from quinone A to plastoquinone ($\psi_0/(1 - \psi_0)$); (D), the equilibrium constant for the redox reactions between PS II and PS I ($\psi_{E0}/(1 - \psi_{E0})$); (E), electron transport from PQH₂ to the reduction of PS I end electron acceptors (RE_0/RC); (F), the contribution of PS I reducing its end acceptors ($\delta_{R0}/(1 - \delta_{R0})$); (G), reaction center II density within the antenna chlorophyll bed of PS II (RC/ABS); (H), contribution or partial performance due to the light reactions for primary photochemistry (TR_0/DI_0), in *Phaeodactylum tricornutum* following a 48 h exposure to a glyphosate-based herbicide formulation in different concentrations (mean \pm s.d., $n = 3$, different letters indicate significant differences at $p < 0.05$).

3.3. Diatom Pigment Composition

Overall, the highest glyphosate-based herbicide concentration ($500 \mu\text{g L}^{-1}$) elicited significant increases in pigment concentrations (Figure 5).

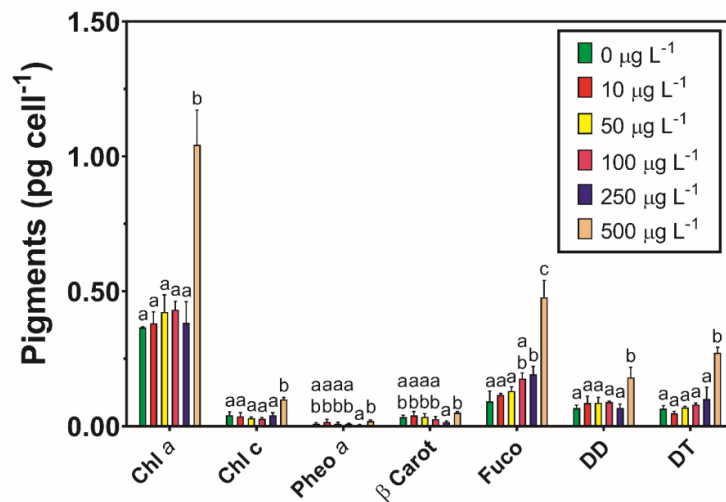


Figure 5. Pigment profile content (chlorophyll *a* (Chl *a*), chlorophyll *c* (Chl *c*), pheophytin *a* (Pheo *a*), β carotene (β Carot), fucoxanthin (Fuco), diadinoxanthin (DD), and diatoxanthin (DT)) in *Phaeodactylum tricornutum* following a 48 h exposure to a glyphosate-based herbicide formulation in different concentrations (mean ± s.d., n = 3, different letters indicate significant differences at *p* < 0.05).

3.4. Diatom Antioxidant Enzymes

The total protein content in *P. tricornutum* only showed a significant increase at the highest glyphosate-based herbicide concentration (500 μg L⁻¹) (Figure 6A). Regarding the antioxidant enzymes CAT, APX, and SOD (Figure 6B–D), only the latter showed statistical differences and only at the highest glyphosate-based herbicide concentration (500 μg L⁻¹), where activity decreased significantly.

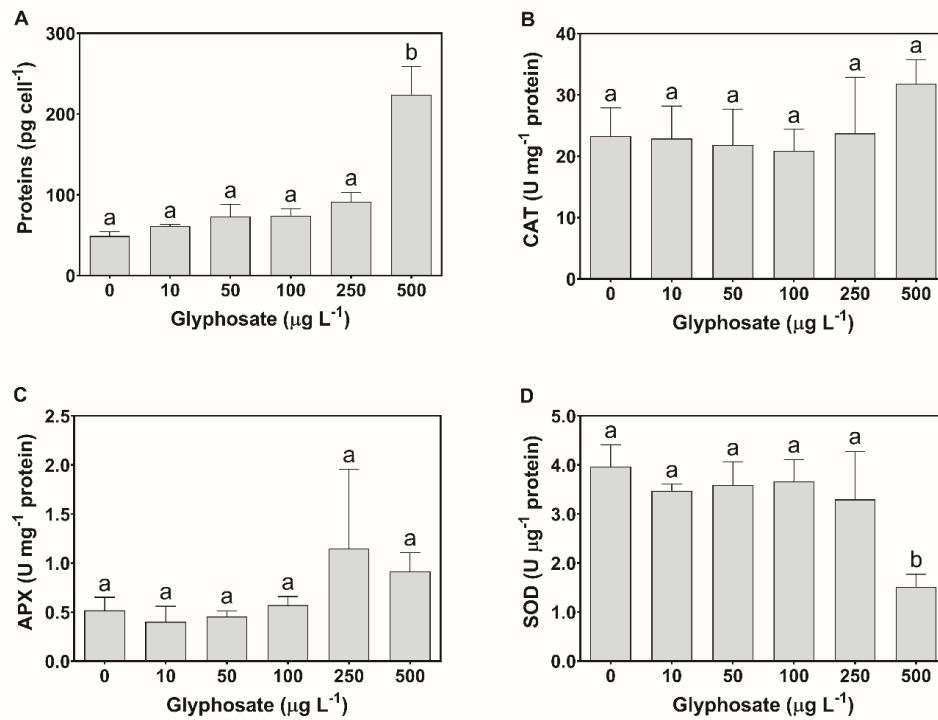


Figure 6. Protein content (A), catalase (CAT, B), ascorbate peroxidase (APX, C), and superoxide dismutase (SOD, D) enzymatic activities in *Phaeodactylum tricornutum* following a 48 h exposure to a glyphosate-based herbicide formulation in different concentrations (mean ± s.d., n = 3, different letters indicate significant differences at *p* < 0.05).

3.5. Diatom Lipid Peroxidation and Fatty Acid Profile

Lipid peroxidation in *P. tricornutum* increased greatly after being subjected to the two highest glyphosate-based herbicide concentrations (250 and 500 $\mu\text{g L}^{-1}$) (Figure 7).

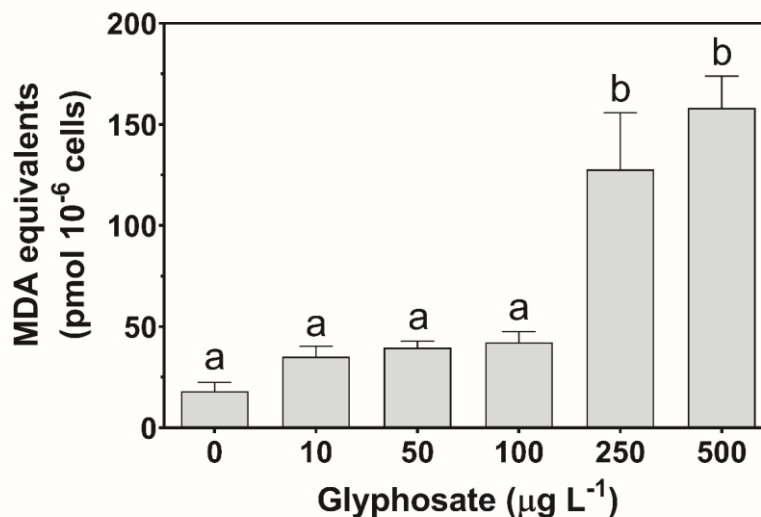


Figure 7. Lipid peroxidation quantification, measured as malondialdehyde (MDA) equivalents, in *Phaeodactylum tricornutum* following a 48 h exposure to a glyphosate-based herbicide formulation in different concentrations (mean \pm s.d., $n = 3$, different letters indicate significant differences at $p < 0.05$).

The total fatty acid content of *P. tricornutum* increased about two-fold after exposure to the two highest concentrations of the herbicide formulation for 48 h (Figure 8). The fatty acid (FA) profile was also affected by the same concentrations (Figure 9).

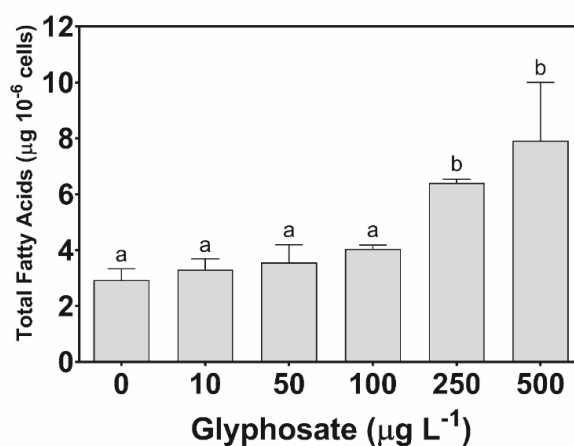


Figure 8. Total fatty acid content in *Phaeodactylum tricornutum* following a 48 h exposure to a glyphosate-based herbicide formulation in different concentrations (mean \pm s.d., $n = 3$, different letters indicate significant differences at $p < 0.05$).

The eicosapentaenoic acid (EPA) (20:5), an omega-3 fatty acid, showed a significant decrease at the highest glyphosate-based herbicide concentration, whilst triunsaturated hexadecatrienoic acid (16:3), exclusively present in plastidial lipids, increased (Figure 9).

While no significant differences were observed for FA major classes and derived ratios (Supplementary Figures S3 and S4), a tendency for an increase was observed in the omega 6/omega 3 ratio at the two highest concentrations of herbicide formulation (Supplementary Figure S5).

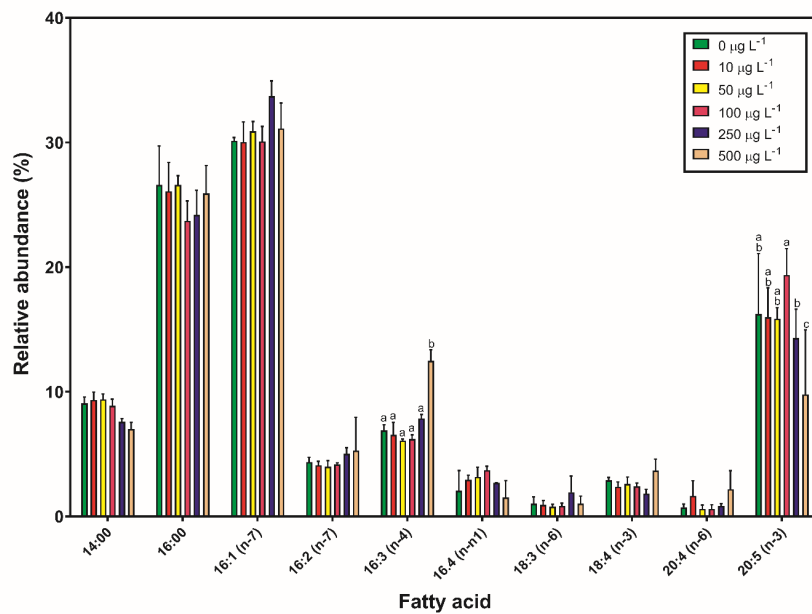


Figure 9. Fatty acid profile in *Phaeodactylum tricornutum* following a 48 h exposure to a glyphosate-based herbicide formulation in different concentrations (mean \pm s.d., $n = 3$, different letters indicate significant differences at $p < 0.05$).

3.6. Energy Balance

Regarding the energy balance in *P. tricornutum*, the two highest glyphosate-based herbicide concentrations (250 and 500 $\mu\text{g L}^{-1}$) triggered an increase in Ea (within proteins, lipids, and carbohydrates) and ETS, with CEA also higher in those concentrations and statistically different from control and the lowest glyphosate-based herbicide concentration (10 $\mu\text{g L}^{-1}$) but not from intermediate ones (50 and 100 $\mu\text{g L}^{-1}$) (Figure 10).

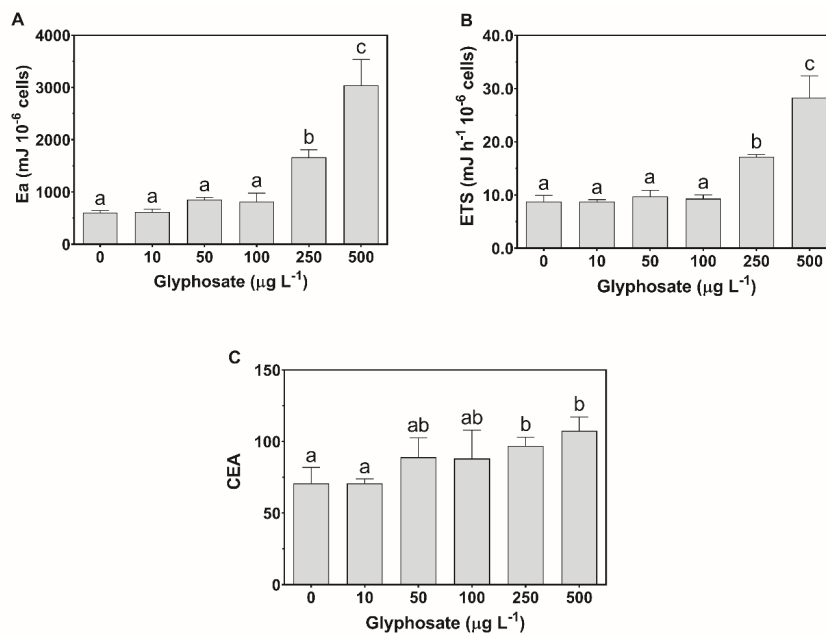


Figure 10. Energy balance ((A), energy available (Ea); (B), energy consumption rate (ETS); (C), cellular energy allocation (CEA)) in *Phaeodactylum tricornutum* following a 48 h exposure to glyphosate-based herbicide formulation in different concentrations (mean \pm s.d., $n = 3$, different letters indicate significant differences at $p < 0.05$).

3.7. Multivariate Classification

The multivariate CAP analysis using the Kautsky plot, the pigment composition, and the fatty acid profile of *P. tricornutum* cultures exposed to different glyphosate-based herbicide concentrations revealed two different classifications, clearly dependent on the class of biomarkers applied (Figure 11).

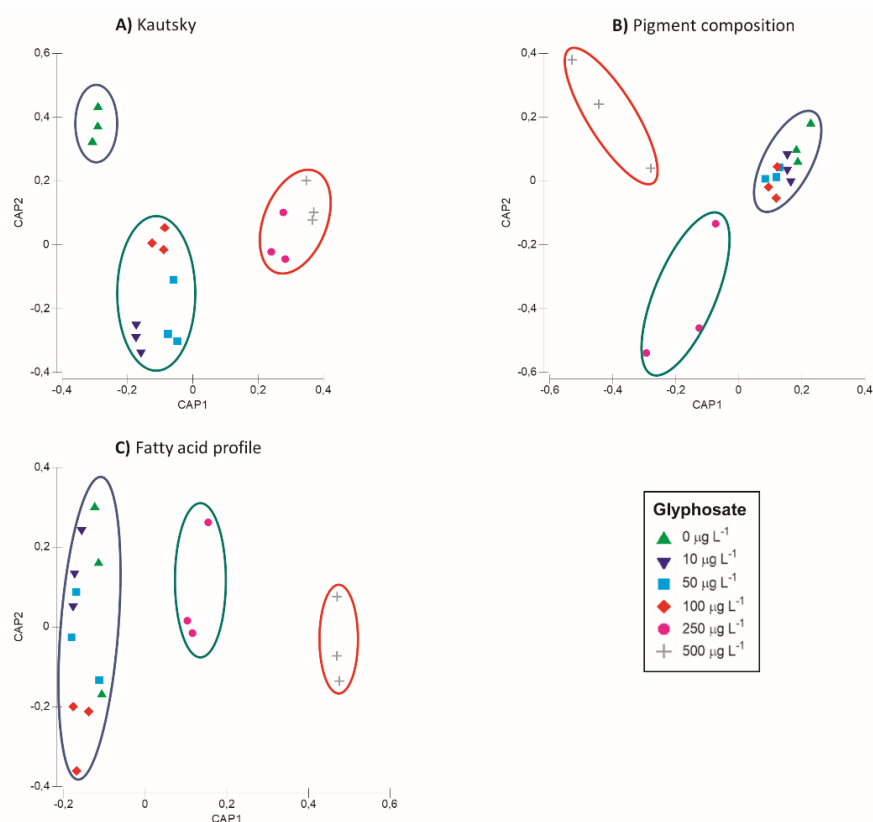


Figure 11. Canonical analysis plot based on the Kautsky plot (A), pigment composition (B), and fatty acid profile (C) of *Phaeodactylum tricornutum* following a 48 h glyphosate-based herbicide formulation in different concentrations. Ellipses group samples with lower statistical distance based on Euclidean resemblances.

The CAP plot based on the Kautsky plot allowed the separation in three groups: (1) Control, (2) intermediate glyphosate-based herbicide concentrations (10 to 100 $\mu\text{g L}^{-1}$), and (3) highest glyphosate-based herbicide concentrations (250 and 500 $\mu\text{g L}^{-1}$). On the other hand, the CAP analysis of both pigment composition and fatty acid profile produced similar group classifications, clustering in one group control and intermediate glyphosate-based herbicide concentrations (10 $\mu\text{g L}^{-1}$ to 100 $\mu\text{g L}^{-1}$) but separating into distinct groups the highest glyphosate-based herbicide concentrations (250 and 500 $\mu\text{g L}^{-1}$). The Kautsky plot CAP analysis produced the model with the highest overall classification efficiency (72.2%), followed by the pigment content (61.1%) and lastly the fatty acid profile (44.4%).

4. Discussion

The cell density of *Phaeodactylum tricornutum* decreased with exposure to increasing concentrations of glyphosate-based herbicide concentrations with an EC_{50} of 225.9 $\mu\text{g L}^{-1}$. A comparable effect was observed with similar glyphosate concentrations in freshwater diatoms *Gomphonema parvulum*, *Achnanthes minutissima*, and *Amphora veneta* [19] and some cyanobacteria such as *Planktothrix agardhii* and *Microcystis aeruginosa* [70]. Besides the potential direct effect of this herbicide, it is also possible that, due to its chelating properties, the bioavailability of macro- and micronutrients (e.g., divalent cations including calcium, magnesium, manganese, and iron) is reduced, limiting growth [71]. Current

environmental concentrations and the unrestrained use of glyphosate-based products pose a continued threat to diatom populations and likely bottom-up effects in trophic webs that need to be further explored. The effect of the glyphosate-based mixture on *P. tricornutum* was very clear in several photochemical-related variables and showed lower photosynthetic efficiency, particularly at the highest concentrations of the glyphosate-based herbicide. However, exposure to the highest concentration led to an increase in all pigments, particularly in chlorophyll content, in opposition to what has been described for higher plants [72] and is likely a compensatory mechanism by which the diatoms counteract the lower efficiency of the affected reaction centers. In other works [73–77], an increase in chlorophyll *a* concentration was observed in algae communities exposed to low concentrations of atrazine (10 to 32 $\mu\text{g L}^{-1}$) but not at higher concentrations. Thus, this rise in chlorophyll content associated with the increase in fucoxanthin content may provide cells with the ability to counteract the decrease in the number of RC/CS, and therefore an increase in the efficiency of each RC available to trap photons occurs. In *P. tricornutum*, the PS II light-harvesting complex is composed of the fucoxanthin-chlorophyll protein (FCP) complex, which may deregulate the light-harvesting capacity, increasing both the ability to trap photons and the number of RC available for reduction [46]. However, there was an increase in photoprotective pigments, including β -carotene, diadinoxanthin, and diatoxanthin, which often allows the cells to increase the energy dissipation through non-photochemical processes, preventing possible photoinhibitory events. Moreover, a decrease in the contribution of the dark reactions from Q_A^- to plastocyanin reinforces the hypothesis that glyphosate at higher concentrations may have nefarious effects on the responses studied, mainly at the ETC level in diatoms [45].

Regarding the fatty acid analyses, the most striking result was the significant increase in the total lipid content, which was nearly twice that in control when cells were exposed to the two highest herbicide concentrations. These increases in microalgae lipid contents are commonly associated with stress conditions, such as nutrient limitation or temperature increase [16,46]. Additionally, exposure to these higher glyphosate-based herbicide concentrations also induced changes in the fatty acid profile of the diatom. It is interesting to note that concomitantly with the increase in the contents of photosynthetic pigments there was also a rise in the relative amounts of 16:3 present in plastidial lipids, namely monogalactosidiacylglycerol, one of the most abundant thylakoid lipids [46]. Changes in chloroplastidial FA composition can lead to alterations of the redox potential [76]. Quinones in the ETC are more efficient at the functional level, showing higher QA reduction rates, which follows the mildly positive effects observed at the PS I level. On the other hand, there was a decrease in the percentage of EPA, usually abundant in all *P. tricornutum* membranes, which likely translates into an impairment in membrane-dependent reactions, such as transmembrane transport and thylakoid and mitochondrial electron transport. This could explain the lower culture growth rates at the highest glyphosate-based herbicide concentrations. Moreover, since EPA is an omega-3 fatty acid with key roles in vertebrate biochemistry, the decrease in its contents (reflected also in the omega-6/omega-3 ratio) is likely to negatively affect the nutritional quality of the diatom, inevitably impacting all the trophic web [77]. Nevertheless, because *P. tricornutum* showed tolerance to the lowest glyphosate-based herbicide concentrations (up to 100 $\mu\text{g L}^{-1}$) and is still able to remain alive in the highest concentrations, this can lead to biomagnification induced by glyphosate-based herbicides, leading to a possible vector of contamination and bioaccumulation. This should be addressed in future works due to the possibility of contamination within the trophic web.

If, on one hand, photosynthetic and photoprotective antioxidant pigments increased, which may be also partly explained by the lack of changes in CAT and APX activities, on the other hand, the decreased activity of SOD can lead to the accumulation of lethal superoxide anions and consequent oxidation of several biological components, such as proteins, lipids, and EPA fatty acid [78]. However, a decrease in the energy transduction at the ETC, from Q_A to plastoquinone, originated a lethal situation of increased redox accumulation in the affected photosystems [79]. Therefore, the energy reaching the PS I was lower, although the effectiveness of the energy transport from PQH_2 to the PS I was not affected (RE_0/RC), and even increased under the highest glyphosate-based herbicide concentrations.

Yet, a severe shift in the redox equilibrium between photosystems towards the PS II ($\psi_{E0}/(1 - \psi_{E0})$) was still observed, decreasing the redox potential reaching the PS I, and thus impairing the light and dark reactions of photosynthesis and the renewal of substrates in the PS I [45].

Nevertheless, the available energy (E_a) increased in the highest glyphosate-based herbicide concentrations, particularly at $500 \mu\text{g L}^{-1}$, probably due to an increase in lipid and protein concentrations. The increase in E_a has been observed in green algae, which accumulated energy reserves as a response to environmental stress [64,80,81]. A possible explanation could be related to the need for algae to counteract the increase in energy expenditure, as observed in the present study. Therefore, following a similar pattern as E_a , the energy consumption demonstrated by the mitochondrial ETS of *P. tricornutum* increased significantly at the highest concentrations, reaching a 300% increase in the highest concentration relative to control. This increase in energy consumption has been observed in other microalgae [65]. Nonetheless, the E_a was higher than the ETS, which led to a slight increase of the CEA in the highest concentrations but only allowing a differentiation of the highest concentrations from the control and the lowest concentrations. This increase in CEA may reflect a higher impairment in mitochondria functioning relative to chloroplast functioning that can ultimately impact the latter due to biophysical disturbances [82]. While these energy balances appear to indicate an increase in the energy available for growth or cell division, the highest glyphosate-based herbicide concentrations inhibited diatom culture growth. Based on this data, stress forces the energy to shift from photosynthesis into energy consumption. This may change photosynthetic electron pathways, leading to E_a downregulation and an increase in ETS to avoid carbon waste, as a strategy to handle an excess of metabolic energy. There are different metabolic pathways under which energy spillover can be managed, but current relevant knowledge is still very scarce [32].

The CAP analyses were very efficient in the assessment of the effects of the glyphosate-based herbicide on the photochemistry, pigment composition, and lipid metabolism of *P. tricornutum*, as well as on the potential of these metabolic features as toxicity biomarkers. However, only the use of bio-optical techniques (e.g., Kautsky plot) allowed an efficient identification of all the different glyphosate-based herbicide exposure treatments (control, low, intermediate, and high concentrations). As in previous studies, multivariate analysis efficiently classified groups subjected to different exposure levels, in comparison to the often-used univariate analysis [12,45,69]. While glyphosate is the main component of Roundup[®], other substances are also in its composition and it is of great interest in future works to assess synergies and/or antagonisms between the herbicide formulation versus glyphosate in its pure form, comparing the values to those measured in the habitats.

5. Conclusions

Glyphosate-based pesticides, particularly at high concentrations, have a clear effect on several metabolic pathways in marine diatoms (changes in pigment profile, photosynthetic impairment, and decreased antioxidant capacity). Even though photoprotective mechanisms were induced, membrane damage still occurred. These facts highlight the application of pulse amplitude modulated chlorophyll fluorescence bio-optical methods as a promising tool for inclusion in ecotoxicological studies with several advantages relative to the classical biochemical approaches, namely fast data acquisition, lower monetary costs, and a high number of variables obtained while ensuring a high degree of accuracy. Thus, bio-optical tools appear as a fast, inexpensive, and reliable method for toxicophenomic assessment of the impacts of this widespread pesticide in marine diatoms, with a clear dose-response pattern. Moreover, the high volume of data produced by these bio-optical techniques can be efficiently applied in multivariate analysis, providing a classification with a high degree of accuracy. With this in mind, PAM fluorometry appears to be a promising tool for inclusion in ecotoxicological studies aiming towards a possible use in long-range detection through satellite imagery in a global chemical pollution-monitoring network.

Supplementary Materials: The following are available online at <http://www.mdpi.com/2076-3417/10/21/7391/s1>, Figure S1: Photosystem II and ETC related photochemical traits, Figure S2: Rapid light curves and derived parameters, Figure S3: Major fatty acids classes, Figure S4: Fatty acid ratios, Figure S5: Omega 6 to omega 3 fatty acid ratio, Table S1: Fluorometric analysis parameters and their description.

Author Contributions: Conceptualization, B.D., V.F.F. and P.R.-S.; methodology, B.D.; formal analysis, R.C.d.C. and B.D.; investigation, R.C.d.C., E.F. and S.C.N.; data curation, R.C.d.C.; writing—original draft preparation, R.C.d.C.; writing—review and editing, E.F., A.R.M., M.T.C., S.C.N., M.F.L.L., I.C., J.C.M., P.R.-S., V.F.F., B.D.; supervision, B.D.; project administration, B.D.; funding acquisition, B.D. All authors have read and agreed to the published version of the manuscript.

Funding: This research was funded by Fundação para a Ciência e a Tecnologia (FCT) via project grants PTDC/CTA-AMB/30056/2017 (OPTOX), UID/MAR/04292/2019, UID/MULTI/04046/2019. Work was also funded by the Integrated Programme of SR&TD SmartBioR (reference Centro-01-0145-FEDER-000018), co-funded by Centro 2020 program, Portugal 2020, European Union, through the European Regional Development Fund. B. Duarte and V. Fonseca were supported by investigation contracts (CEECIND/00511/2017 and DL57/2016/CP1479/CT0024). P. Reis-Santos was supported by FCT through a postdoctoral grant (SFRH/BPD/95784/2013).

Acknowledgments: The authors would like to thank Caroline Casey and Joana Roma for revising the English language, grammar, punctuation, and spelling of the manuscript.

Conflicts of Interest: The authors declare no conflict of interest.

Abbreviations

ALA	α -linolenic acid;
APX	ascorbate peroxidase;
CAP	Canonical Analysis of Principal Coordinates;
CAT	catalase;
CEA	cellular energy allocation;
DBI	double bond index;
DD	diadinoxanthin;
DHA	docosahexaenoic acid;
DT	diatoxanthin;
Ea	energy available;
Ec	energy consumption;
EC	Effective Concentration;
EFA	essential fatty acids;
EPA	eicosapentaenoic acid;
EPSPS	5-enolpyruvyl-shikimate-3-phosphate synthase;
ETC	electron transport chain;
ETS	electron transport system;
FAME	fatty acids methyl esters;
FCP	fucoxanthin-chlorophyll protein;
LC-PUFA	polyunsaturated fatty acids;
LOEC	Lowest Observed Effect Concentration;
MDA	malondialdehyde;
NOEC	No Observed Effect Concentration;
OEC	oxygen-evolving complexes;
PAM	Pulse Amplitude Modulated;
PS I	photosystem I;
PS II	photosystem II;
RC	reaction centers;
RLC	rapid light curves;
SOD	superoxide dismutase

References

1. Gavrilesco, M.; Demnerová, K.; Aamand, J.; Agathos, S.; Fava, F. Emerging pollutants in the environment: Present and future challenges in biomonitoring, ecological risks and bioremediation. *New Biotechnol.* **2015**, *32*, 147–156. [[CrossRef](#)] [[PubMed](#)]

2. Thomaidis, N.S.; Asimakopoulos, A.G.; Bletsou, A.A. Emerging contaminants: A tutorial mini-review. *Glob. NEST J.* **2012**, *14*, 72–79.
3. EUROSTAT. Available online: https://ec.europa.eu/eurostat/statistics-explained/index.php?title=Archive:Chemicals_production_statistics&oldid=199190 (accessed on 7 September 2020).
4. CAS REGISTRY Keeps Pace with Rapid Growth of Chemical Research, Registers 60 Millionth Substance. Available online: <https://www.acs.org/content/acs/en/pressroom/newsreleases/2011/may/cas-registrysm-k-pace-with-rapid-growth-of-chemical-research-registers-60-millionth-substance.html> (accessed on 7 September 2020).
5. Duke, S.O.; Powles, S.B. Glyphosate: A once-in-a-century herbicide. *Pest. Manag. Sci.* **2008**, *64*, 319–325. [[CrossRef](#)] [[PubMed](#)]
6. Van Straalen, N.M.; Legler, J. Decision-making in a storm of discontent. *Science* **2018**, *360*, 958–960. [[CrossRef](#)]
7. Steinrucken, H.C.; Amrhein, N. The herbicide glyphosate is a potent inhibitor of 5-enolpyruvyl-shikimic-acid 3-phosphate synthase. *Biochem. Biophys. Res. Commun.* **1980**, *94*, 1207–1212. [[CrossRef](#)]
8. Tan, S.; Evans, R.; Singh, B. Herbicidal inhibitors of amino acid biosynthesis and herbicide-tolerant crops. *Amino Acids* **2006**, *30*, 195–204. [[CrossRef](#)]
9. Annett, R.; Habibi, H.R.; Hontela, A. Impact of glyphosate and glyphosate-based herbicides on the freshwater environment. *J. Appl. Toxicol.* **2014**, *34*, 458–479. [[CrossRef](#)]
10. Mercurio, P.; Flores, F.; Mueller, J.F.; Carter, S.; Negri, A.P. Glyphosate persistence in seawater. *Mar. Pollut. Bull.* **2014**, *85*, 385–390. [[CrossRef](#)]
11. Mercurio, P.; Mueller, J.F.; Eaglesham, G.; Flores, F.; Negri, A.P. Herbicide persistence in seawater simulation experiments. *PLoS ONE* **2015**, *10*, e0136391. [[CrossRef](#)]
12. Cabrita, M.T.; Duarte, B.; Gameiro, C.; Godinho, R.M.; Caçador, I. Photochemical features and trace element substituted chlorophylls as early detection biomarkers of metal exposure in the model diatom *Phaeodactylum tricorutum*. *Ecol. Indic.* **2018**, *95*, 1038–1052. [[CrossRef](#)]
13. Cabrita, M.T.; Gameiro, C.; Utkin, A.B.; Duarte, B.; Caçador, I.; Cartaxana, P. Photosynthetic pigment laser-induced fluorescence indicators for the detection of changes associated with trace element stress in the diatom model species *Phaeodactylum tricorutum*. *Environ. Monit. Assess.* **2016**, *188*, 285. [[CrossRef](#)] [[PubMed](#)]
14. Castro-Bugallo, A.; González-Fernández, Á.; Guisande, C.; Barreiro, A. Comparative responses to metal oxide nanoparticles in marine phytoplankton. *Arch. Environ. Con. Toxicol.* **2014**, *67*, 483–493. [[CrossRef](#)] [[PubMed](#)]
15. Cabrita, M.T.; Brito, P.; Caçador, I.; Duarte, B. Impacts of phytoplankton blooms on trace metal recycling and bioavailability during dredging events in the Sado estuary (Portugal). *Mar. Environ. Res.* **2020**, *153*, 104837. [[CrossRef](#)] [[PubMed](#)]
16. Guschina, I.A.; Harwood, J.L. Algal lipids and effect of the environment on their biochemistry. In *Lipids in Aquatic Ecosystems*; Kainz, M., Brett, M.T., Arts, M.T., Eds.; Springer: New York, NY, USA, 2009; pp. 1–24. [[CrossRef](#)]
17. Smedbol, É.; Lucotte, M.; Labrecque, M.; Lepage, L.; Juneau, P. Phytoplankton growth and PSII efficiency sensitivity to a glyphosate-based herbicide (Factor 540®). *Aquat. Toxicol.* **2017**, *192*, 265–273. [[CrossRef](#)]
18. Pérez, G.; Torremorell, A.; Mugni, H.; Rodríguez, P.; Vera, M.S.; Nascimento, M.; Allende, L.; Bustingorry, J.; Escaray, R.; Ferraro, M.; et al. Effects of the herbicide Roundup on freshwater microbial communities: A mesocosm study. *Ecol. Appl.* **2007**, *17*, 2310–2322. [[CrossRef](#)]
19. Vera, M.S.; Lagomarsino, L.; Sylvester, M.; Pérez, G.L.; Rodríguez, P.; Mugni, H.; Sinistro, R.; Ferraro, M.; Bonetto, C.; Zagarese, H.; et al. New evidences of Roundup® (glyphosate formulation) impact on the periphyton community and the water quality of freshwater ecosystems. *Ecotoxicology* **2010**, *19*, 710–721. [[CrossRef](#)]
20. Stachowski-Haberkorn, S.; Becker, B.; Marie, D.; Haberkorn, H.; Coroller, L.; Broise, D. Impact of Roundup on the marine microbial community, as shown by an in situ microcosm experiment. *Aquat. Toxicol.* **2008**, *89*, 232–241. [[CrossRef](#)]
21. Marchand, M.; Tissier, C. L'analyse du risque chimique en milieu marin: L'approche méthodologique européenne. *Environ. Risques Sante* **2007**, *6*, 127–141. [[CrossRef](#)]
22. Minguez, L.; Pedelucq, J.; Farcy, E.; Ballandonne, C.; Budzinski, H.; Halm-Lemeille, M.P. Toxicities of 48 pharmaceuticals and their freshwater and marine environmental assessment in north-western France. *Environ. Sci. Pollut. Res.* **2016**, *23*, 4992–5001. [[CrossRef](#)]

23. Cabrita, M.T. Phytoplankton community indicators of changes associated with dredging in the Tagus estuary (Portugal). *Environ. Pollut.* **2014**, *191*, 17–24. [[CrossRef](#)]
24. Cabrita, M.T.; Raimundo, J.; Pereira, P.; Vale, C. Immobilised *Phaeodactylum tricornutum* as biomonitor of trace element availability in the water column during dredging. *Environ. Sci. Pollut. Res.* **2014**, *21*, 3572–3581. [[CrossRef](#)] [[PubMed](#)]
25. Claessens, M.; Vanhaecke, L.; Wille, K.; Janssen, C.R. Emerging contaminants in Belgian marine waters: Single toxicant and mixture risks of pharmaceuticals. *Mar. Pollut. Bull.* **2013**, *71*, 41–50. [[CrossRef](#)] [[PubMed](#)]
26. Gameiro, C.; Utkin, A.B.; Cartaxana, P.; Marques da Silva, J.; Matos, A.R. The use of laser induced chlorophyll fluorescence (LIF) as a fast and non-destructive method to investigate water deficit in *Arabidopsis*. *Agric. Water Manag.* **2016**, *164*, 127–136. [[CrossRef](#)]
27. Denman, K.L.; Gargett, A.E. Time and space scales of vertical mixing and advection of phytoplankton in the upper ocean. *Limnol. Oceanogr.* **1983**, *28*, 801–815. [[CrossRef](#)]
28. Basu, S.; Mackey, K.R.M. Phytoplankton as key mediators of the biological carbon pump: Their responses to a changing climate. *Sustainability* **2018**, *10*, 869. [[CrossRef](#)]
29. Armbrust, E.V.; Berges, J.A.; Bowler, C.; Green, B.R.; Martinez, D.; Putnam, N.H.; Zhou, S.; Allen, A.E.; Apt, K.E.; Bechner, M.; et al. The genome of the diatom *Thalassiosira pseudonana*: Ecology, evolution, and metabolism. *Science* **2004**, *306*, 79–86. [[CrossRef](#)] [[PubMed](#)]
30. Hockin, N.L.; Mock, T.; Mulholland, F.; Kopriva, S.; Malin, G. The response of diatom central carbon metabolism to nitrogen starvation is different from that of green algae and higher plants. *Plant Physiol.* **2012**, *158*, 299–312. [[CrossRef](#)]
31. Smith, S.R.; Abbriano, R.M.; Hildebrand, M. Comparative analysis of diatom genomes reveals substantial differences in the organization of carbon partitioning pathways. *Algal Res.* **2012**, *1*, 2–16. [[CrossRef](#)]
32. Wagner, H.; Jakob, T.; Fanesi, A.; Wilhelm, C. Towards an understanding of the molecular regulation of carbon allocation in diatoms: The interaction of energy and carbon allocation. *Philos. Trans. R. Soc. B* **2017**, *372*, 20160410. [[CrossRef](#)]
33. Sayanova, O.; Mimouni, V.; Ulmann, L.; Morant-Manceau, A.; Pasquet, V.; Schoefs, B.; Napier, J.A. Modulation of lipid biosynthesis by stress in diatoms. *Philos. Trans. R. Soc. B* **2017**, *372*, 20160407. [[CrossRef](#)]
34. Arts, M.T.; Ackman, R.G.; Holub, B.J. Essential fatty acids in aquatic ecosystems: A crucial link between diet and human health and evolution. *Can. J. Fish. Aquat. Sci.* **2001**, *58*, 122–137. [[CrossRef](#)]
35. Van West, D.; Maes, M. Polyunsaturated fatty acids in depression. *Acta Neuropsych.* **2003**, *15*, 15–21. [[CrossRef](#)] [[PubMed](#)]
36. Wiktorowska-Owczarek, A.; Berezińska, M.; Nowak, J. PUFAs: Structures, metabolism and functions. *Adv. Clin. Exp. Med.* **2015**, *24*, 931–941. [[CrossRef](#)]
37. Mateos-Naranjo, E.; Redondo-Gómez, S.; Cox, L.; Cornejo, J.; Figueroa, M.E. Effectiveness of glyphosate and imazamox on the control of the invasive cordgrass *Spartina densiflora*. *Ecotoxicol. Environ. Saf.* **2009**, *72*, 1694–1700. [[CrossRef](#)] [[PubMed](#)]
38. Inderjit; Kaushik, S. Effect of herbicides with different modes of action on physiological and cellular traits of *Anabaena fertilissima*. *Paddy Water Environ.* **2010**, *8*, 277–282. [[CrossRef](#)]
39. Diaz-Vivancos, P.; Driscoll, S.P.; Bulman, C.A.; Ying, L.; Emami, K.; Treumann, A.; Mauve, C.; Noctor, G.; Foyer, C.H. Perturbations of amino acid metabolism associated with glyphosate-dependent inhibition of shikimic acid metabolism affect cellular redox homeostasis and alter the abundance of proteins involved in photosynthesis and photorespiration. *Plant Physiol.* **2011**, *157*, 256–268. [[CrossRef](#)] [[PubMed](#)]
40. Gomes, M.P.; Le Manac’h, S.G.; Hénault-Ethier, L.; Labrecque, M.; Lucotte, M.; Juneau, P. Glyphosate-dependent inhibition of photosynthesis in willow. *Front. Plant. Sci.* **2017**, *8*, 207. [[CrossRef](#)]
41. Duarte, B.; Prata, D.; Matos, A.R.; Cabrita, M.T.; Caçador, I.; Marques, J.C.; Cabral, H.N.; Reis-Santos, P.; Fonseca, V.F. Ecotoxicity of the lipid-lowering drug bezafibrate on the bioenergetics and lipid metabolism of the diatom *Phaeodactylum tricornutum*. *Sci. Total Environ.* **2019**, *650*, 2085–2094. [[CrossRef](#)] [[PubMed](#)]
42. Santos, D.; Duarte, B.; Caçador, I. Unveiling Zn hyperaccumulation in *Juncus acutus*: Implications on the electronic energy fluxes and on oxidative stress with emphasis on non-functional Zn-chlorophylls. *J. Photochem. Photobiol. B Biol.* **2014**, *140*, 228–239. [[CrossRef](#)]
43. Consalvey, M.; Perkins, R.G.; Paterson, D.M.; Underwood, G.J.C. PAM fluorescence: A beginner’s guide for benthic diatomists. *Diatom Res.* **2005**, *20*, 1–22. [[CrossRef](#)]

44. Anjum, N.A.; Duarte, B.; Caçador, I.; Sleimi, N.; Duarte, A.C.; Pereira, E. Biophysical and biochemical markers of metal/metalloid-impacts in salt marsh halophytes and their implications. *Front. Environ. Sci.* **2016**, *4*, 24. [[CrossRef](#)]
45. Duarte, B.; Pedro, S.; Marques, J.C.; Adão, H.; Caçador, I. *Zostera noltii* development probing using chlorophyll a transient analysis (JIP-test) under field conditions: Integrating physiological insights into a photochemical stress index. *Ecol. Indic.* **2017**, *76*, 219–229. [[CrossRef](#)]
46. Feijão, E.; Gameiro, C.; Franzitta, M.; Duarte, B.; Caçador, I.; Cabrita, M.T.; Matos, A.R. Heat wave impacts on the model diatom *Phaeodactylum tricornerutum*: Searching for photochemical and fatty acid biomarkers of thermal stress. *Ecol. Indic.* **2017**, *95*, 1026–1037. [[CrossRef](#)]
47. Tomlin, C.D.S. Glyphosate. In *The Pesticide Manual: A World Compendium*, 14th ed.; British Crop Protection Council: Hampshire, UK, 2006; pp. 545–548.
48. Scribner, E.A.; Battaglin, W.A.; Gilliom, R.J.; Meyer, M.T. *Concentrations of Glyphosate, Its Degradation Product, Aminomethylphosphonic Acid, and Glufosinate in Ground and Surface-Water, Rainfall, and Soil Samples Collected in the United States, 2001–2006*; Scientific Investigations Report: 2007–5122; U.S. Geological Survey: Reston, VA, USA, 2007.
49. Struger, J.; Thompson, D.; Staznik, B.; Martin, P.; McDaniel, T.; Marvin, C. Occurrence of glyphosate in surface waters of southern Ontario. *Bull. Environ. Contam. Toxicol.* **2008**, *80*, 378–384. [[CrossRef](#)] [[PubMed](#)]
50. Coupe, R.H.; Kalkhoff, S.J.; Capel, P.D.; Gregoire, C. Fate and transport of glyphosate and aminomethylphosphonic acid in surface waters of agricultural basins. *Pest Manag. Sci.* **2012**, *68*, 16–30. [[CrossRef](#)] [[PubMed](#)]
51. Giroux, I. *Présence de Pesticides dans l'Eau au Québec: Portrait et Tendances dans les Zones de Maïs et de Soya–2011 à 2014*; Ministère du Développement Durable, de l'Environnement et de la Lutte Contre les Changements Climatiques, Direction du Suivi de L'état de L'environnement: Quebec City, QC, Canada, 2015; ISBN 978-2-550-73603-5.
52. Guillard, R.R.L.; Ryther, J.H. Studies of marine planktonic diatoms: I. *Cyclotella nana* Hustedt, and *Detonula confervacea* (Cleve) Gran. *Can. J. Microbiol.* **1962**, *8*, 229–239. [[CrossRef](#)]
53. OECD. OECD guidelines for the testing of chemicals. Freshwater alga and cyanobacteria, growth inhibition test. *Organ. Econ. Coop. Dev.* **2011**, 1–25. [[CrossRef](#)]
54. Santos-Ballardo, D.U.; Rossi, S.; Hernández, V.; Gómez, R.V.; Rendón-Unceta, M.; Caro-Corrales, J.; Valdez-Ortiz, A. A simple spectrophotometric method for biomass measurement of important microalgae species in aquaculture. *Aquaculture* **2015**, *448*, 87–92. [[CrossRef](#)]
55. Kim Tiam, S.; Fauvelle, V.; Morin, S.; Mazzella, N. Improving toxicity assessment of pesticide mixtures: The use of polar passive sampling devices extracts in microalgae toxicity tests. *Front. Microbiol.* **2016**, *7*, 1388. [[CrossRef](#)]
56. Kupper, H.; Seibert, S.; Aravind, P. A fast, sensitive and inexpensive alternative to analytical pigment HPLC: Quantification of chlorophylls and carotenoids in crude extracts by fitting with Gauss-peak-spectra. *Anal. Chem.* **2007**, *79*, 7611–7627. [[CrossRef](#)]
57. Bradford, M. A rapid and sensitive method for the quantification of microgram quantities of protein utilizing the principle of protein-dye-binding. *Anal. Biochem.* **1976**, *72*, 248–254. [[CrossRef](#)]
58. Teranishi, Y.; Tanaka, A.; Osumi, M.; Fukui, S. Catalase activities of hydrocarbon-utilizing *Candida* yeast. *Agric. Biol. Chem.* **1974**, *38*, 1213–1220. [[CrossRef](#)]
59. Tiryakioglu, M.; Eker, S.; Ozkutlu, F.; Husted, S.; Cakmak, I. Antioxidant defense system and cadmium uptake in barley genotypes differing in cadmium tolerance. *J. Trace Elem. Med. Biol.* **2006**, *20*, 181–189. [[CrossRef](#)]
60. Marklund, S.; Marklund, G. Involvement of superoxide anion radical in the autoxidation of pyrogallol and a convenient assay for superoxide dismutase. *Eur. J. Biochem.* **1974**, *47*, 464–469. [[CrossRef](#)]
61. Heath, R.L.; Packer, L. Photoperoxidation in isolated chloroplasts. *Arch. Biochem. Biophys.* **1968**, *125*, 189–198. [[CrossRef](#)]
62. De Coen, W.M.; Janssen, C.R. The use of biomarkers in *Daphnia magna* toxicity testing. IV. Cellular energy allocation: A new biomarker to assess the energy budget of toxicant-stressed *Daphnia* populations. *J. Aquat. Ecosyst. Stress Recovery* **1997**, *6*, 43–55. [[CrossRef](#)]
63. De Coen, W.M.; Janssen, C.R. The missing biomarker link: Relationships between effects on the cellular energy allocation biomarker of toxicant-stressed *Daphnia magna* and corresponding population characteristics. *Environ. Toxicol. Chem.* **2003**, *22*, 1632–1641. [[CrossRef](#)]

64. Aderemi, A.O.; Novais, S.C.; Lemos, M.F.; Alves, L.M.; Hunter, C.; Pahl, O. Oxidative stress responses and cellular energy allocation changes in microalgae following exposure to widely used human antibiotics. *Aquat. Toxicol.* **2018**, *203*, 130–139. [[CrossRef](#)]
65. Gnaiger, E. Calculation of energetic and biochemical equivalents of respiratory oxygen consumption. In *Polarographic Oxygen Sensors. Aquatic and Physiological Applications*; Gnaiger, E., Forstner, H., Eds.; Springer: Berlin, Germany, 1983; pp. 337–345. [[CrossRef](#)]
66. King, F.D.; Packard, T.T. Respiration and the activity of the respiratory electron transport system in marine zooplankton. *Limn. Ocean.* **1975**, *20*, 849–854. [[CrossRef](#)]
67. Verslycke, T.; Ghekiere, A.; Janssen, C.R. Seasonal and spatial patterns in cellular energy allocation in the estuarine mysid *Neomysis integer* (Crustacea: Mysidacea) of the Scheldt estuary (The Netherlands). *J. Exp. Mar. Biol. Ecol.* **2004**, *306*, 245–267. [[CrossRef](#)]
68. Clarke, K.R.; Gorley, R.N. *PRIMER v6: User Manual/Tutorial*; Prim: Plymouth, UK, 2006; p. 192. [[CrossRef](#)]
69. Duarte, B.; Carreiras, J.; Pérez-Romero, J.A.; Mateos-Naranjo, E.; Redondo-Gómez, S.; Matos, A.R.; Marques, J.C.; Caçador, I. Halophyte fatty acids as biomarkers of anthropogenic-driven contamination in Mediterranean marshes: Sentinel species survey and development of an integrated biomarker response (IBR) index. *Ecol. Indic.* **2018**, *87*, 86–96. [[CrossRef](#)]
70. Saxton, M.A.; Morrow, E.A.; Bourbonniere, R.A.; Wilhelm, S.W. Glyphosate influence on phytoplankton community structure in Lake Erie. *J. Great Lakes Res.* **2011**, *37*, 683–690. [[CrossRef](#)]
71. Mertens, M.; Höss, S.; Neumann, G.; Afzal, J.; Reichenbecher, W. Glyphosate, a chelating agent—Relevant for ecological risk assessment? *Environ. Sci. Pollut. Res.* **2018**, *25*, 5298–5317. [[CrossRef](#)]
72. Gomes, M.P.; Smedbol, E.; Chalifour, A.; Hénault-Ethier, L.; Labrecque, M.; Lepage, L.; Lucotte, M.; Juneau, P. Alteration of plant physiology by glyphosate and its by-product aminomethylphosphonic acid: An overview. *J. Exp. Bot.* **2014**, *65*, 4691–4703. [[CrossRef](#)]
73. Lynch, T.; Johnson, H.E.; Adams, W.J. Impact of atrazine and hexachlorobiphenyl on the structure and function of model stream ecosystems. *Environ. Toxicol. Chem.* **1985**, *4*, 399–413. [[CrossRef](#)]
74. Tang, J.X.; Hoagland, K.D.; Siegfried, B.D. Differential toxicity of atrazine to selected freshwater algae. *Bull. Environ. Contam. Toxicol.* **1997**, *59*, 631–637. [[CrossRef](#)] [[PubMed](#)]
75. Seguin, F.; Druart, J.C.; Le Cohu, R. Effects of atrazine and nicosulfuron on periphytic diatom communities in freshwater outdoor lentic mesocosms. *Ann. Limnol. Int. J. Limnol.* **2001**, *37*, 3–8. [[CrossRef](#)]
76. Kern, J.; Guskov, A. Lipids in photosystem II: Multifunctional cofactors. *J. Photochem. Photobiol. B Biol.* **2011**, *104*, 19–34. [[CrossRef](#)]
77. Khan, M.; Rahman, M.M.; Zaman, S.; Jahangir, T.A.; Razu, M.H. Omega-3 polyunsaturated fatty acids from algae. In *Chapter 5—Recent Advances in Microalgal Biotechnology*; Liu, J., Sun, Z., Gerken, H., Eds.; OMICS Group eBooks: Foster City, CA, USA, 2015. [[CrossRef](#)]
78. Foyer, C.H.; Noctor, G. Ascorbate and glutathione: The heart of the redox hub. *Plant Physiol.* **2011**, *155*, 2–18. [[CrossRef](#)]
79. Havurinne, V.; Tyystjärvi, E. Action spectrum of photoinhibition in the diatom *Phaeodactylum tricornerutum*. *Plant Cell Physiol.* **2017**, *58*, 2217–2225. [[CrossRef](#)]
80. Cheng, D.; He, Q. Assessment of environmental stresses for enhanced microalgal biofuel production—An overview. *Front. Energy Res.* **2014**, *2*, 26. [[CrossRef](#)]
81. Paes, C.R.P.S.; Faria, G.R.; Tinoco, N.A.B.; Castro, D.J.F.A.; Barbarino, E.; Lourenço, S.O. Growth, nutrient uptake and chemical composition of *Chlorella* sp. and *Nannochloropsis oculata* under nitrogen starvation. *Lat. Am. J. Aquat. Res.* **2016**, *44*, 275–292. [[CrossRef](#)]
82. Gomes, M.P.; Juneau, P. Oxidative stress in duckweed (*Lemna minor* L.) induced by glyphosate: Is the mitochondrial electron transport chain a target of this herbicide? *Environ. Pol.* **2016**, *218*, 402–409. [[CrossRef](#)]

Publisher’s Note: MDPI stays neutral with regard to jurisdictional claims in published maps and institutional affiliations.



© 2020 by the authors. Licensee MDPI, Basel, Switzerland. This article is an open access article distributed under the terms and conditions of the Creative Commons Attribution (CC BY) license (<http://creativecommons.org/licenses/by/4.0/>).